

Ultralight-Weight Graphene Aerogels with Extremely High Electrical Conductivity

Lucía dos Santos-Gómez,* José R. García, Miguel A. Montes-Morán,
José Angel Menéndez, Santiago García-Granda, and Ana Arenillas*

The integration of 2D graphene sheets into a porous and macroscopic structure is extremely attractive for application in several electrochemical fields. In this regard, for the first time, the synthesis of 3D graphene aerogels is reported by using a rapid, easy, cost-effective, and scalable at industrial level methodology. These aerogels integrate the intrinsic properties of graphene with a high pore volume. To achieve this ultraporous graphene network, resorcinol/formaldehyde polymer with controllable porosity is employed as a binder and a cross-linker material, and a graphene oxide solution provides the graphene building blocks. Two series of materials with and without catalyst for resorcinol/formaldehyde reaction and with different synthesis conditions and graphene contents are studied. The resulting graphene aerogels present low density, large macroporosity, and electrical conductivity values as high as 852 S m^{-1} , with 97.58% of porosity, which is the highest value of electrical conductivity reported so far in the literature for ultralight-weight graphene aerogels.

materials because their structural, morphological, thermal, and electrical properties can be eventually controlled during the synthesis procedure.^[3,4] This characteristic has allowed the development of a wide variety of materials, i.e., carbon aerogels (CA), with specific applications, such as catalytic supports, thermal insulators, chemical adsorbents, and energy storage materials.^[5,6]

The most significant characteristic of carbon aerogels is that their porous properties, mesoporosity and macroporosity, can be tailored during the synthesis procedure by choosing the adequate reagents and conditions, among which the most prominent are the type of catalyst, pH, concentration, temperature, and time of the different synthesis steps.^[7–9] For example, in the gelation stage of the resorcinol/formaldehyde

1. Introduction

The design of materials with tailored chemical and physical characteristics has rapidly grown in the recent years.^[1,2] Several research studies have been focused on synthetic carbonaceous


(R/F) aerogels, the polycondensation of both molecules produces spherical nodules that crosslink to each other during the curing stage. After that, the empty space between all the nodules becomes pores with a specific size, depending of the size of the nodules, in the drying step. Hence, the porosity can be varied with high precision by controlling the sizes of these nodules, which leads to design aerogels with specific porous texture.^[9] Moreover, the extremely large porosity of the aerogels provides unique characteristics, such as low thermal conductivity, low density, and large specific surface area. Nevertheless, carbon aerogels do not simultaneously possess both large porosity and ultrahigh electrical conductivity, which are normally opposed properties. This is because a high porosity implies an amorphous structure with several defects, besides a well-developed open porous structure, which are not favorable for the transfer of electrons while an ordered and connected carbon structure is required in order to get high electrical conductivity.^[10,11] In this sense, further investigations on highly conductor aerogels are necessary to obtain a combination of both properties in a single material.

On the contrary, ordered carbon materials, such as graphene, present high electron mobility, but, although in some cases it may exhibit large specific surface area, it usually presents low porosity. Thus, the combination of 2D graphene with a binder material to create a 3D carbon material that integrates the intrinsic properties of graphene with a high pore volume has been intensively pursued.^[12–14] Different binder materials, including organic molecules, metal ions, and polymers, have been investigated to create porous graphene aerogels.^[15–18] Because of the low dispersive properties of graphene, graphene

L. dos Santos-Gómez, S. García-Granda
Department of Physical and Analytical Chemistry
Avda. Julián Clavería 8, Campus de El Cristo
Oviedo University–CINN-CSIC
Oviedo 33006, Spain
E-mail: ldsg@uniovi.es

J. R. García
Department of Organic and Inorganic Chemistry
Oviedo University–CINN-CSIC
Oviedo 33006, Spain

M. A. Montes-Morán, J. A. Menéndez, A. Arenillas
Instituto de Ciencia y Tecnología del Carbono
INCAR-CSIC
Francisco Pintado Fe 26, Oviedo 33011, Spain
E-mail: ana.arenillas@csic.es

 The ORCID identification number(s) for the author(s) of this article can be found under <https://doi.org/10.1002/smll.202103407>.

© 2021 The Authors. Small published by Wiley-VCH GmbH. This is an open access article under the terms of the Creative Commons Attribution-NonCommercial-NoDerivs License, which permits use and distribution in any medium, provided the original work is properly cited, the use is non-commercial and no modifications or adaptations are made.

DOI: 10.1002/smll.202103407

oxide (GO) with acceptable solubility is utilized instead of pristine graphene as a building block for constructing 3D graphene networks.^[19–21] The oxygenated groups of the graphene oxide sheets, i.e., hydroxyl, aldehyde, or carboxyl, are the principal covalent linking sites with the binder material. However, the addition of a binder does not always allow to a satisfactory morphology with adequate porosity.

The development of 3D graphene aerogels with controlled porosity and high electrical conductivity is extremely attractive for their application in several fields, especially as electrode materials for electrochemical energy devices such as supercapacitors, batteries, and fuel cells.^[22,23] Moreover, to the best of our knowledge, it has not been prepared graphene aerogels, which possess at the same time both porosity and electrical conductivity high enough to be commercially used.

On the other hand, graphene aerogel manufacturing procedures have to be cost effective, not time consuming and easily scalable at industrial scale. The use of conventional heating techniques in the synthesis of aerogels requires multiple days to obtain the final material.^[24] On the contrary, the gelation process is reduced to a few hours when the microwave radiation is employed as a heating source, obtaining porous aerogels with properties similar to those prepared by the conventional synthesis method.^[25] In this context, microwave-assisted synthesis has resulted to be a very competitive, efficient, and well-established method to prepare carbon aerogels on a large scale, reducing the time and production costs considerably.

Previously, our group has developed graphene-doped carbon xerogels, where the graphene sheets were embedded into the carbonized R/F matrix, and the resulting materials possessed higher conductivity than the nondoped carbon xerogel.^[26,27]

This work utilizes a new and different concept to create a graphene matrix, where the graphene sheets are linked by the carbon polymer. To this end, a rapid and economic microwave synthesis procedure is used to obtain ultralight graphene aerogels which combine both a greatly porous structure and an excellent electrical conductivity. To achieve this combination, an R/F polymer with controllable porosity is employed as the binder material and a GO solution (cheaper than pristine graphene) as building blocks to create an ultraporous graphene network with remarkable electrical conductivity. Graphene aerogels containing different amounts of graphene are synthesized. Moreover, two series of materials are defined according to the use (or not) of NaOH as a catalyst for the R/F polymerization. The CA obtained are labeled as CA-*D*-C and CA-*D*-unC for the catalyzed and uncatalyzed series, respectively, where *D* indicates the dilution ratio of GO suspension used in the synthesis process. The catalyzed graphene aerogel prepared with the concentrated GO suspension is labeled as CA-60·2-C and the catalyzed R/F aerogel (without graphene) as CA-C. The study also includes the complete structural, morphological, and electrical characterizations of the graphene aerogels.

2. Results and Discussion

2.1. Optimization of the Drying Method

Solvent elimination is a critical step in the drying procedure of graphene aerogels, affecting to their microstructure and physical

properties such as porosity, density, and electrical conductivity. Two different strategies, to remove the water from the organic aerogels (OA), are studied. Representative photos of two organic samples, i.e., OA-C and OA-20-C, dried by thermal treatment (TT) and freeze-drying method (FD) are shown in Figure S1a–d (Supporting Information). On the one hand, aerogels dehydrated by TT are more compact since the solvent is evaporated creating a vapor/liquid interface in the internal surface of the material. Thus, elevated surface tensions are generated due to the capillary forces, which produce the partial or total collapse of the structure.^[28–30] This phenomenon is also reflected on the color of the aerogels, i.e., OA-C dried by TT (Figure S1a, Supporting Information) is darker than that with the same composition dried by FD (Figure S1b, Supporting Information). On the contrary, the FD method allows maintaining the morphology of the as-synthesized organic aerogel, since the solvent is sublimated much more slowly, preserving the highly porous structure of the organic aerogel.^[31,32] Figure S1e–h (Supporting Information) shows scanning electron microscopy (SEM) images of OA-C and OA-20-C dried by both procedures, also confirming the higher porosity of the FD aerogels. In addition, the porous structure is more elevated in graphene aerogels (Figure S1g,h, Supporting Information) than in R/F ones (Figure S1e,f, Supporting Information). Therefore, only graphene aerogels dehydrated by FD are further investigated.

2.2. Structure and Composition of the Graphene Aerogels

The polycondensation reactions of resorcinol and formaldehyde molecules with the oxygenated groups of the graphene oxide sheets allow the formation of porous and well-connected networks (Figure 1a–d). For that, not only attach the R/F polymer with the graphene oxide surface, but also hydroxyl, aldehyde, and carboxyl groups of the graphene oxide sheets react with the formaldehyde and resorcinol molecules via covalent crosslinking (Figure 1d). The resulting structures of the aerogels possess a good robustness due to such covalent unions.

Figure 1e displays the X-ray diffraction (XRD) patterns of CA-C and CA-*D*-C (*D* = 20, 40, 60, and 60·2) series as a representative example of all graphene aerogels prepared. Two broad peaks are observed for the R/F aerogel without graphene, CA-C, at 20.5° and 44.1° (2θ), which are assigned to the (002) and (10) reflections of carbons with low structural order, respectively.^[33–35] The (002) peak narrows as the amount of reduced graphene increases in the graphene aerogels, with its maximum shifting to higher 2θ values (up to 24.5°). At the same time, the intensity of the (10) reflection weakens with the graphene content. As a result, the XRD pattern of CA-60·2-C resembles that of pure reduced GO (rGO).^[36,37]

The total amount of rGO (hereafter referred to as “graphene”) presented in the carbon aerogels was estimated by assuming that the GO is totally reduced to graphene over the carbonization procedure, as has been shown by XRD analysis. It is important to notice that the wt% of graphene contained in the carbon aerogels is just an approximation since such assumption is necessary to do the estimation. The mass percentages of the carbonized R/F frameworks and graphene were determined by thermogravimetric (TGA) analysis, using the same heating rate than that utilized during the carbonization process. The

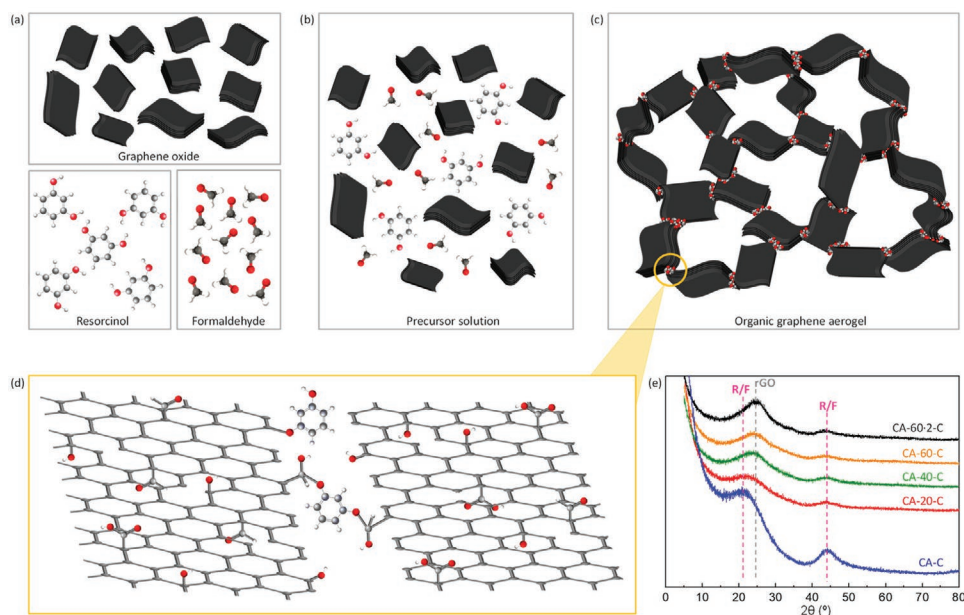


Figure 1. a–d) Schematic representation of the formation of organic graphene aerogels. e) XRD patterns for the CA-C and CA-D-C ($D = 20, 40, 60,$ and $60\cdot 2$) graphene aerogels.

estimated percentages of graphene for the catalyzed and uncatalyzed series are shown in **Table 1**, ranging from 6 to 28 wt% and from 11 to 40 wt% for CA-20-C to CA-60-2-C and for CA-40-unC to CA-200-unC, respectively.

2.3. Morphology of the 3D Network

Figure 2 shows photographs and SEM images of the CA-40-unC graphene aerogel at different magnifications. The ultralightness of the materials allows them to stay onto the surface of a dandelion, without damaging or deforming it (**Figure 2a**). Graphene aerogels present a highly porous morphology created

by the assembly of 2D graphene sheets. This microstructure is quite different from that of the interconnected microspheres of R/F aerogels (**Figure S1**, Supporting Information). Most of the graphene aerogel has empty space, where graphene sheets are randomly connected between them, creating a 3D network with large pores (**Figure 2c,d**). R/F nanoparticles decorate the surfaces of these graphene networks, being clearly distinguishable at higher magnification SEM images (**Figure 2e**). These images suggest that R/F particles are homogeneously extended onto the graphene framework, acting as a connecting link and allowing graphene sheets to remain united. This may be due to the fact that the polymerization of the R/F precursor is promoted by the functional groups of the GO sheets, forming covalent unions

Table 1. Textural properties of the aerogels obtained in this work with different wt% of graphene.

Composition	Graphene [wt%]	Porosity [%]	Density [mg cm^{-3}]	S_{BET} [$\text{m}^2 \text{g}^{-1}$]	V_{T} [$\text{cm}^3 \text{g}^{-1}$]	V_{meso} [$\text{cm}^3 \text{g}^{-1}$]	V_{macro} [$\text{cm}^3 \text{g}^{-1}$]	Pore [μm]	
Catalyzed	CA-C	0	85.49	303	732	2.478	0.011	2.467	35.8
	CA-20-C	6	92.80	148	667	6.455	0.006	6.449	1.4
	CA-40-C	11	93.23	132	389	8.062	0.063	7.999	5.3
	CA-60-C	16	96.06	82	422	12.289	0.024	12.265	13.1
	CA-60-2-C	28	92.36	136	–	–	–	–	–
Uncatalyzed	CA-40-unC	11	97.71	63	764	15.107	0.191	14.916	5.6
	CA-60-unC	16	98.45	44	599	19.768	0.270	19.498	6.3
	CA-80-unC	21	98.66	47	651	30.297	0.290	30.007	12.2
	CA-100-unC	25	99.24	47	605	37.221	0.248	36.973	18.8
	CA-120-unC	28	99.45	48	1320	39.483	0.298	39.186	22.9
	CA-140-unC	32	99.32	39	351	42.362	0.472	39.011	48.9
	CA-160-unC	35	99.58	42	496	37.938	0.459	37.479	22.1
	CA-180-unC	37	93.58	52	388	44.227	0.296	43.931	62.6
	CA-200-unC	40	97.58	73	385	37.835	0.354	37.481	96.1

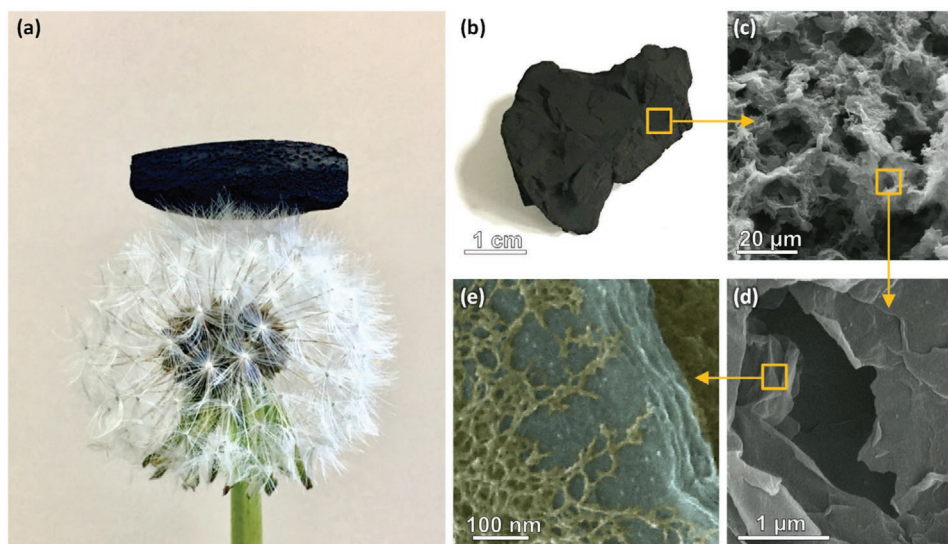


Figure 2. a) Photograph of graphene aerogel standing on the top of a dandelion and b) photograph and c–e) SEM images of CA-40-unC graphene aerogel at different magnifications.

between them.^[12] After that, R/F and GO are simultaneously carbonized, and both the R/F bonds and the reduction of the GO functionalities blend these two compounds, yielding a porous and ultralight 3D framework. This robust blending is observed by high-resolution transmission electron microscopy (HRTEM), where the connection between two different structures, amorphous and crystalline corresponding to the R/F polymer and graphene sheets, respectively, is clearly distinguishable (Figure S2, Supporting Information).

According to the SEM images, the amount of graphene in the aerogel seems to be higher than that previously calculated by TGA analysis (Table 1), where more than half of the weight of the sample is assigned to carbonized R/F polymer. This may be explained by the different densities of R/F and rGO, ≈ 1.9 and ≈ 0.1 g cm⁻³, respectively,^[38] and also because the graphene structures are very light but they occupy a lot of volume compared to the gel matrix which is more compact. Thus, the aerogels possess a large amount of graphene volume with respect to R/F polymer, as confirmed by SEM images.

The morphology of the 3D network slightly changes with the graphene content, as shown in **Figure 3**. Catalyzed aerogels with a low amount of graphene present structures formed by individual and randomly distributed graphene sheets with a high degree of carbonized R/F coating (Figure 3a). These sheets are linked by the carbonized R/F polymer, forming the 3D framework. However, when the graphene content increases, the degree of carbonized R/F coating decreases, producing the graphene sheets that gradually roll and fold and, consequently, the porosity of the network increases (Figure 3b,c). In addition, the framework architecture of the aerogels is more uniform as the graphene content increases, especially, that of CA-60-C, since the graphene sheets tend to align, creating a robust and more ordered structure. On the contrary, when the amount of graphene is too high (CA-60.2-C), not all graphene sheets are covered by the carbonized R/F polymer. These uncoated sheets remain trapped inside the 3D network and the porosity of the aerogel decreases (Figure 3d).

On the other hand, the resulting microstructure for the uncatalyzed series presents natural sea sponge shape morphology, with larger macropores and smoother and thinner wall structure than the catalyzed ones (**Figure 4**). This series displays similar trends than the catalyzed aerogels, increasing the pore size and the lightness of the materials with the graphene content.

2.4. Porous Properties

The qualitative assessment of the porosity of graphene aerogels by SEM was confirmed when calculating the porosity percentage and the density of the samples (Table 1). Both the catalyzed and uncatalyzed series are extremely light and have low densities. The porosity percentages range from 85.49% to 96.06% for the catalyzed series and 97.71% to 99.58% for the uncatalyzed one. The porosity percentage of the catalyzed aerogels increased with the graphene content. However, the CA-60.2-C aerogel does not follow the same trend of the series, presenting porosity and density values similar to those samples with lower graphene content, as previously observed by SEM. Thus, the optimal porous properties for the catalyzed series are achieved by CA-60-C material. Higher graphene content produces a decrease in the porosity since the number of graphene sheets is too elevated in comparison with the amount of R/F polymer.

The porosity percentages of the uncatalyzed series are even higher. The lightest graphene aerogel corresponds to CA-160-unC composition, which also presents one of the lowest values of density, 42 mg cm⁻³. Such an increase of porosity of the uncatalyzed series may be explained by both the pH of the precursor solution due to the absence of catalyst and the volume of GO dispersion added. During the R/F polycondensation reaction, the resorcinol is responsible for the formation of the nodules, and the formaldehyde reinforces the aerogel by creating a more interconnected and branched structure. The pH affects the speed of the reaction since the lower the pH

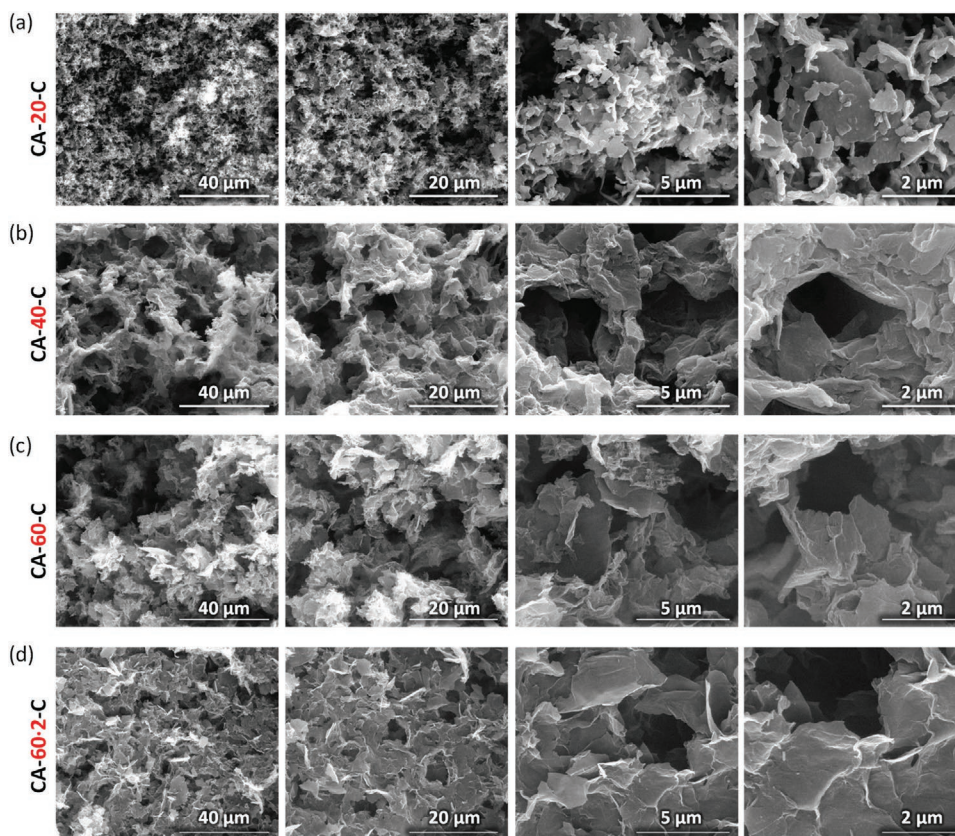


Figure 3. SEM images of the CA-D-C (*D* values of a) 20, b) 40, c) 60, and d) 60-2) graphene aerogels at different magnifications.

is, the slower the anions of resorcinol are created. As a consequence, the higher number of nodules with larger size is formed, which increases the porosity. Moreover, the volume of solvent added influences the separation between nodules, so, increasing the volume of GO dispersion produces an increase

of the distance between them. The combination of these two parameters makes a higher porosity of the uncatalyzed series due to their lower pH and also justifies the increase of the porosity among the both series due to the large amount of GO suspension employed.

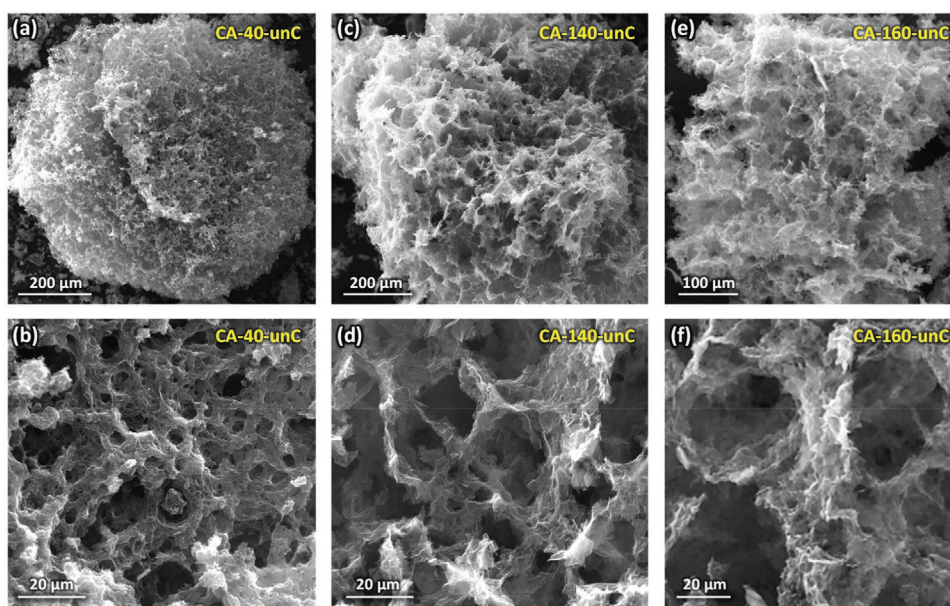


Figure 4. SEM images at different magnifications of a,b) CA-40-unC, c,d) CA-140-unC, and e,f) CA-160-unC, respectively.

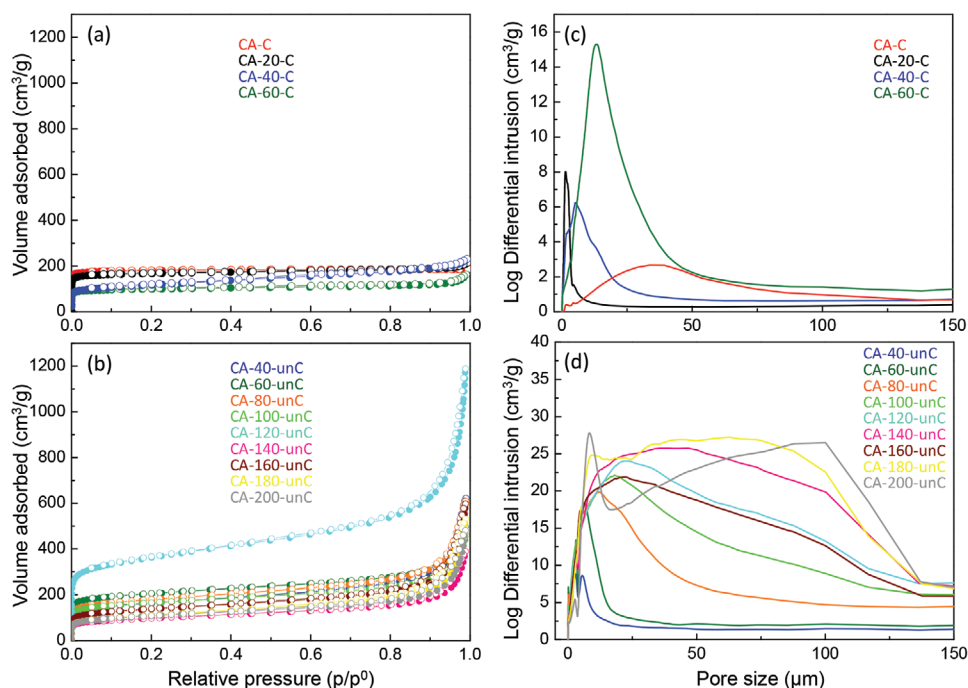


Figure 5. a,b) N₂ adsorption–desorption isotherms and c,d) pore size distributions obtained from mercury porosimetry for the catalyzed and uncatalyzed graphene aerogels.

The porous properties of both series of graphene aerogels were further studied by N₂ adsorption at cryogenic temperature. **Figure 5a,b** shows the N₂ adsorption–desorption isotherms of the catalyzed and uncatalyzed compounds, respectively. Isotherms of all graphene aerogels are related to reversible type II isotherms of the International Union of Pure and Applied Chemistry (IUPAC) classification, which correspond to macroporous solids. The isotherms show a low increase of N₂ adsorption at low relative pressures, indicating a low volume of micropores. Then, the amount of N₂ adsorbed increases linearly with the relative pressure. When the relative pressure approaches to 1, there is a significant increase of the amount of N₂ adsorbed. This behavior is characteristic of macroporous materials. The shapes of the isotherms are similar for all samples, although the uncatalyzed aerogels show a sharper increase at high relative pressure, indicating a higher macroporosity than the catalyzed ones. Nevertheless, all samples present moderate Brunauer–Emmett–Teller (BET) specific surface areas (i.e., >350 m² g⁻¹). According to the results obtained, it seems that the microporosity and, therefore, the surface area decrease from values ≈750 m² g⁻¹, with the increase of graphene oxide. Therefore, the microporosity is mainly due to the carbonized R/F polymer.

The determination of pore volumes by N₂ adsorption is not too precise for materials with wide pores. Therefore, mercury porosimetry was also carried out to calculate the size and volume of macro- and mesopores in these materials (Table 1). It is worth mentioning that the increase of the GO content also produces certain compressibility of the samples, and that may interfere on the interpretation of Hg porosimetry data. The pore size distributions of the catalyzed and uncatalyzed aerogels are shown in **Figure 5c,d**. The average pore size of the aerogels increases with the graphene content. CA-D-unC

series possess larger pore size than the CA-D-C one, and thus a higher macroporosity, which is in agreement with the N₂ adsorption tests shown in **Figure 5a,b**. Moreover, the pore distribution is wider among the two series when the amount of graphene increases. This fact may be due to the lower degree of R/F coating of the samples with elevated graphene content, which produces that graphene sheets roll up and, consequently, larger and less homogeneous pore sizes are produced. The incorporation of graphene to the aerogels mainly influences on the macropore volume (Table 1), while there is not a clear trend on the mesoporosity. According to the values obtained from mercury porosimetry, there is an increase of macropore volume with the graphene content, these types of pores being the main contribution to the total pore volume. There were no observed variations, either the compression properties or the mechanical resistance between the CA-C and the different graphene aerogels. The only changes observed were related to the porosity since the pore volume increased with the dilution ratio, which decreased the density of the samples (Table 1).

2.5. Electrical Measurements

Electrical conductivity values obtained by the four-probe method for the catalyzed and uncatalyzed graphene aerogels are represented in **Figure 6**. The electrical conductivity of both series increases with the graphene content due to the morphology of their 3D frameworks, ranging from 23 to 852 S m⁻¹ for the CA-C and CA-60-C compounds of the catalyzed aerogels, and from 80 to 719 S m⁻¹ for the CA-40-unC and CA-200-unC compounds of the uncatalyzed ones, respectively. Aerogels with a large amount of graphene present a continuous and

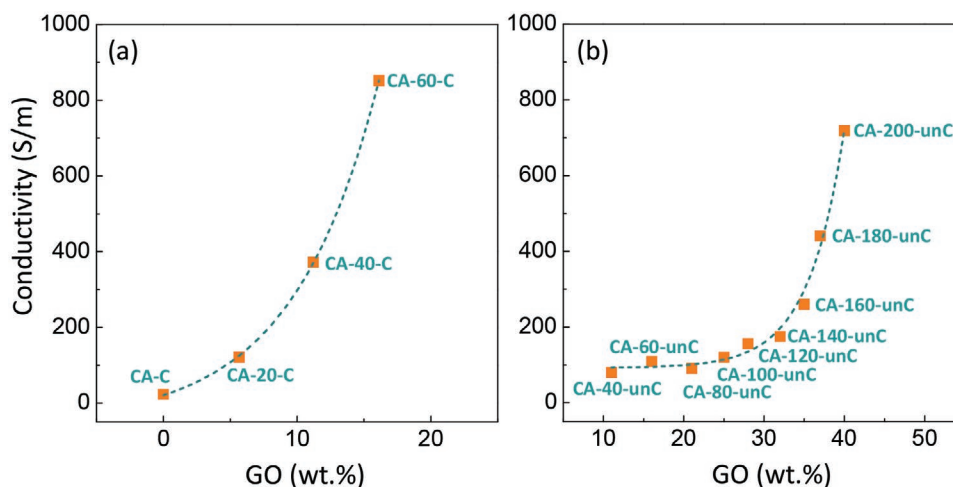


Figure 6. Influence of wt% of graphene in the electrical conductivity values for the a) catalyzed and b) uncatalyzed series of graphene aerogels.

well-connected graphene sheets' structure, which is vital to get high electrical conductivity since the electron transfer is easier.^[39] However, in aerogels with low graphene content and large amount of carbonized R/F polymer, the graphene sheets are not linked enough to allow the electrical percolation limit to be achieved (i.e., the percolation threshold is not reached). This is the reason why the conductivity value of CA-20-C graphene aerogel is more similar to that of the RF aerogel without graphene while CA-60-C possesses an extremely high conductivity value 37 times higher than that of the CA-C aerogel. Therefore, it is important to highlight that the graphene content in the aerogel needs to be high enough to allow a good connection between the graphene sheets.

The conductivities of the uncatalyzed aerogels are lower than those of the catalyzed series (Figure 6b). For example, CA-40-C possesses a conductivity value of 372 S m⁻¹ while the analogous uncatalyzed aerogel, CA-40-unC, only presents a value of 80 S m⁻¹, assuming that both samples have similar graphene contents. Moreover, the conductivity differences are more pronounced for the CA-60-C and CA-60-unC, with values of 852 and 109 S m⁻¹, respectively. This is related to the porosity and the volume of macropores, which are more elevated for the uncatalyzed samples, producing a lower degree of percolation between the graphene sheets and decreasing the electrical conductivity.

Furthermore, the loss of the oxygenated functionalities of the GO during the carbonization process, as confirmed by XRD, also improves the electrical conductivity of the aerogels. This is largely due to the fact that the elimination of the functional groups effectively restores the sp² conjugation in these regions with the concomitant appearance of the π - π interaction between the adjacent carbon atoms.^[40,41,43] Moreover, more interactions are also created in the crosslinking sites between the graphene sheets and the R/F polymer, which bonds the graphene sheets together and creates a unique and highly porous 3D network with exceptionally high electrical conductivity.

The highest values of electrical conductivity were achieved by CA-60-C and CA-200-unC samples of the catalyzed and uncatalyzed series with 852 and 719 S m⁻¹ and 96.06% and 97.58% of porosity, respectively. It is worth noting that these values are among the highest ones published in the literature so far

for graphene aerogels (Table 2). Such aerogels also present the highest electrical conductivity values as a function of the density (Figure 7). In addition, the usually reported graphene aerogels present high electrical conductivity but low porosity and vice versa. Other graphene aerogels reported, with pore sizes predominately sub 20 nm, need elevated thermal treatments (2500 °C) to achieve high electrical conductivity (about 550 S m⁻¹), which significantly increases the production costs at industrial scale.^[50] Nevertheless, the graphene aerogels prepared in this work exhibit simultaneously both large porosity and extremely high conductivity, making them suitable for a wide range of applications in different areas, especially on electrochemical devices, i.e., lithium-ion batteries and sensors.

Table 2. Electrical conductivity values (measured by Four Point Probe, K-FPP) and porous properties of the aerogels obtained in this work in comparison with the literature.

Composition	S_{BET} [m ² g ⁻¹]	Density [mg cm ⁻³]	Porosity [%]	K-FPP [S m ⁻¹]	Ref.
CA-60-C	422	82	96.06	852	This work
CA-200-unC	385	73	97.58	719	This work
Graphene aerogel	244	150	–	133	[42]
Graphene aerogel	512	86	–	63	[44]
Graphene aerogel	584	–	–	87	[12]
Graphene aerogel	–	2	–	17	[44]
Graphene aerogel	–	7	–	16	[45]
Graphene aerogel (1500 °C)	441	–	–	157	[46]
Carbon sphere aerogels	609	51	–	695	[47]
Cu ₁ /Cu _x O@rGO aerogel	48	–	97.70	430	[48]
Graphene-doped carbon xerogel	1556	–	–	310	[26]
Graphene aerogel composite	–	16	–	25	[49]
Graphene aerogel	345	45	–	550	[50]

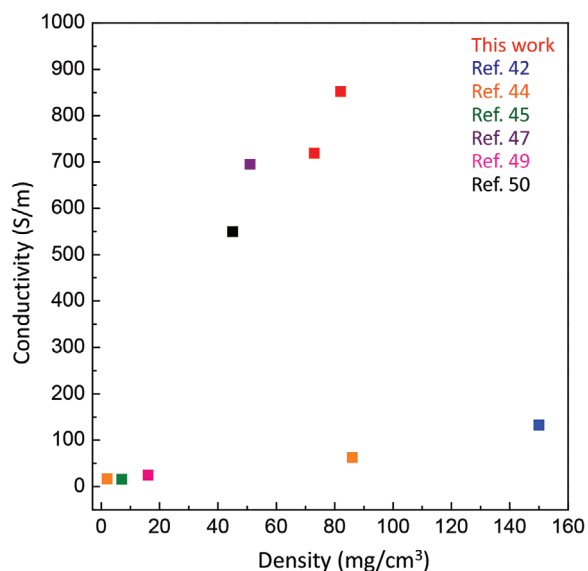


Figure 7. Electrical conductivity values versus density of CA-60-C and CA-200-unC reported in this work and those reported in the literature.

3. Conclusions

In summary, new graphene aerogels have been successfully developed by using graphene oxide dispersions and resorcinol/formaldehyde polymer. Two series of materials without and with catalyst have been studied. The graphene sheets of these aerogels are partially covered by the carbonized R/F polymer, which acts as a connecting link between them, creating a seamlessly interconnected 3D network. The perfect connection of the graphene sheets in this type of network simultaneously gives the aerogel outstanding porous properties and ultrahigh electrical conductivity. The catalyzed series may present a small amount of catalyst but higher electrical conductivity with lower quantity of graphene, which makes these aerogels less expensive than the uncatalyzed one. On the contrary, the uncatalyzed series is characterized by the absence of catalysts but the higher amount of graphene is necessary to achieve the same values of conductivity than the catalyzed one, which makes them more expensive. The CA-60-C aerogel presents the best electrical conductivity value, 852 S m^{-1} with 97.58% of porosity. This is the highest value of electrical conductivity reported so far for a graphene aerogel with such an extremely large porosity. That high electrical conductivity is due to the large degree of percolation between the graphene sheets, allowing an easier electron transfer. In addition, the synthesis technique employed is scalable and versatile at industrial scale, and may be a strategy to fabricate 3D graphene structures with preconformed shapes and excellent properties, which should enable several applications of these materials in diverse areas.

4. Experimental Section

Synthesis of Aerogels: Catalyzed and uncatalyzed graphene aerogels were prepared by the R/F polycondensation reaction following an analogous synthetic procedure described in previous works.^[9,51] First

of all, R/F aerogel (without graphene) was synthesized by dissolving resorcinol (Indspec, 99%) in distilled water under constant stirring for 1 h. After that, stoichiometric amount of formaldehyde commercial solution (Ercros, 37 wt% in water, 10–15% methanol) was incorporated, and the resulting mixture was stirred for 5 min to ensure a uniform distribution of all reagents. The dilution ratio used was 10, which was related to the molar ratio between the total solvent added to the precursor solution and the amount of reactants. The pH was adjusted to 5 by adding the NaOH solution (1 mol L^{-1}), which acted as the catalyst for the polycondensation reaction. Then, the solution was heated at $85 \text{ }^\circ\text{C}$ for 3 h in a microwave oven in order to accelerate the gelation process. This procedure was much faster than other gelation routes which last several days.^[24]

Catalyzed graphene aerogels were prepared with an identical procedure except that the distilled water was replaced by a commercial graphene oxide (GO) suspension (Applnano Solutions S.L., 5 mg mL^{-1}). The addition of the GO suspension to the precursor solution modified the initial pH of the mixture (i.e., initial pH of an R/F mixture was ≈ 3.5 vs 1.8 with GO suspension). Therefore, 1 mol L^{-1} of the NaOH solution was used for adjusting the final pH to 5. In this series, the dilution ratio was gradually increased (20, 40, and 60) by decreasing the quantity of R/F and adding higher amount of GO suspension to get an aerogel with the maximum amount of GO. The dilution ratio was calculated by dividing the amount (in mol) of liquid substances (water contained in the GO suspension, water contained in the formaldehyde solution, and methanol contained in the formaldehyde solution) by the amount of the solid ones (GO, resorcinol, and formaldehyde). For instance, for a typical batch at the laboratory, such as the CA-20-C sample, the synthesis procedure was as follows: 18.816 g of resorcinol was dissolved in 168 mL of GO suspension (5 mg mL^{-1}) under stirring. Then, 27.735 g of formaldehyde was added to the solution, and the pH of the initial mixture was measured. The series with different dilution ratio were obtained by the addition of more GO suspension, which means an increase of the GO content in the final sample, and the reduction of resorcinol and formaldehyde. Thus, for the sample CA-60-C, 6.922 g of resorcinol, 198 mL of GO suspension, and 10.203 g of formaldehyde were employed. However, there was a limit of the amount of GO suspension, as at high dilution ratio there was no gelation and a solid material was not obtained. The dilution ratio limit was 60 since no gelation was achieved at higher dilution ratio values. An additional catalyzed graphene aerogel with a dilution ratio of 60 was prepared by using a GO suspension of higher concentration (10 mg mL^{-1}).

Uncatalyzed graphene aerogels were synthesized with the same, previously described process but NaOH solution was not added as catalyst; thus, the pH of the precursor solution was not altered (≈ 1.8). In this series, the dilution ratios used were 40, 60, 80, 100, 120, 140, 160, 180, and 200. No homogeneous gelation was achieved above this maximum dilution ratio.

All the organic aerogels were dehydrated by two processes: i) the water was evaporated by TT in a furnace at $120 \text{ }^\circ\text{C}$ until constant weight, and (ii) the water was sublimated by freeze drying (FD). The freeze-drying procedure was performed by freezing the samples in liquid N_2 and introducing them in the freeze-dryer equipment for 24 h. Finally, the dried organic aerogels were carbonized at $1000 \text{ }^\circ\text{C}$ for 1 h under a N_2 regular flow of 150 mL min^{-1} and a heating rate of $1 \text{ }^\circ\text{C min}^{-1}$ in order to get the CA and reduce the GO to rGO.

Structural, Morphological, and Porous Characterization: All aerogels were studied by XRD with a D8 Advance (Bruker) diffractometer and sealed-tube $\text{Cu K}\alpha 1$ radiation. A Göbel mirror configuration was employed to collect the reflected radiation. The total measurement time was 1 h over 5° – 80° (2θ) angular range. Phase identification was performed with X'Pert HighScore Plus program.^[52]

TGA was carried out on a SDTQ600 analyzer (TA Instruments) under a regular N_2 airflow of 20 mL min^{-1} at a heating rate of $1 \text{ }^\circ\text{C min}^{-1}$ from room temperature to $1000 \text{ }^\circ\text{C}$.

The morphology of the aerogels was examined by SEM (Quanta FEG 650) equipped with an Everhart–Thornley Detector secondary electron detector (Everhart–Thornley), and by HRTEM (JEOL 2100Plus).

The porosity percentage and the density of the samples were determined by using an AccuPyc 1330 pycnometer (Micromeritics) and

a Geopyc 1360 device (Micromeritics). All samples were previously outgassed in a VAcPrep 0.61 device (Micromeritics) at 120 °C for 12 h to eliminate possible physisorbed gases and humidity. N₂ adsorption-desorption isotherms were recorded in a Tristar 3020 instrument (Micromeritics) at -196 °C. Brunauer-Emmett-Teller equation was applied to calculate the BET surface area (S_{BET}). The N₂ adsorbed at the saturation point was used to determine the total pore volume. The meso-macroporous structure was determined by means of mercury porosimetry using an Autopore IV 9500 apparatus (Micromeritics).

Electrical Measurements: The in-plane conductivity of the materials was measured by studying the resistivity of a film made with the samples studied by using the four-probe method and the van der Pauw equation. A four-point probe equipment (SR-4-6L, Everbeing) was employed to do these measurements in air and at room temperature.

The films for these measurements were made by mixing the carbon aerogels with 10 wt% polytetrafluoroethylene (PTFE) as the binder material until that a homogeneous mixture was obtained. After that, the resulting powders were uniaxially pressed into circular films of 1 cm diameter and 200–300 μm thickness, respectively.

Supporting Information

Supporting Information is available from the Wiley Online Library or from the author.

Acknowledgements

This work was supported by the Ministerio de Economía, Industria y Competitividad from Spain (CTQ2017-87820-R and MAT2016-78155-C2-1-R) and Principado de Asturias—FICYT-FEDER (IDI/2018/000118 and IDI/2018/000170). L.d.S.-G. thanks the Ministerio de Ciencia, Innovación y Universidades for her Juan de la Cierva Formación grant (FJC2018-036746-I).

Conflict of Interest

The authors declare no conflict of interest.

Author Contributions

Conceptualization: L.d.S.-G., J.A.M., and A.A.; methodology: L.d.S.-G.; investigation: L.d.S.-G., M.A.M.-M., and A.A.; validation: A.A.; visualization: L.d.S.-G. and A.A.; project administration: M.A.M.-M., J.R.G., S.G.-G., and A.A.; writing of original draft: L.d.S.-G.; review and editing: J.R.G., M.A.M.-M., J.A.M., S.G.-G., and A.A. All authors have read and agreed to the published version of the manuscript.

Data Availability Statement

Research data are not shared.

Keywords

electrical conductivity, graphene aerogels, porosity

Received: June 10, 2021

Revised: July 21, 2021

Published online: September 12, 2021

- [1] X. Lu, M. C. Arduini-Schuster, J. Kuhn, O. Nilsson, J. Fricke, R. W. Pekala, *Science* **1992**, 255, 971.
- [2] A. Feinle, M. S. Elsaesser, N. Huesing, *Chem. Soc. Rev.* **2016**, 45, 3377.
- [3] A. M. Elkhatat, S. A. Al-Muhtaseb, *Adv. Mater.* **2011**, 23, 2887.
- [4] A. C. Pierre, G. M. Pajonk, *Chem. Rev.* **2002**, 102, 4243.
- [5] H. Maleki, *Chem. Eng. J.* **2016**, 300, 98.
- [6] A. C. Pierre, G. M. Pakonk, *Chem. Rev.* **2002**, 102, 4243.
- [7] S. A. Al-Muhtaseb, J. A. Ritter, *Adv. Mater.* **2003**, 15, 101.
- [8] N. Job, R. Pirard, J. Marien, J. P. Pirard, *Carbon* **2004**, 42, 619.
- [9] N. Rey-Raap, J. A. Menéndez, A. Arenillas, *Carbon* **2014**, 78, 490.
- [10] Q. Wang, J. Yan, Z. Fan, *Energy Environ. Sci.* **2016**, 9, 729.
- [11] L. L. Zhang, X. Zhao, M. D. Stoller, Y. Zhu, J. Hengxing, S. Murali, Y. Wu, S. Perales, B. Clevenger, R. S. Ruoff, *Nano Lett.* **2012**, 12, 1806.
- [12] M. A. Worsley, P. J. Pauzaskie, T. Y. Olson, J. Biener, J. H. Satcher, T. F. Baumann, *J. Am. Chem. Soc.* **2010**, 132, 14067.
- [13] C. Lee, X. Wei, J. W. Kysar, J. Hone, *Science* **2008**, 321, 385.
- [14] A. Bianco, Y. Chen, Y. Chen, D. Ghoshal, R. H. Hurt, Y. A. Kim, N. Koratkar, V. Meunier, M. Terrones, *Carbon* **2018**, 132, 785.
- [15] J. Wang, M. Ellsworth, *ECS Trans.* **2009**, 19, 241.
- [16] H. Bai, C. Li, X. Wang, G. Shi, *J. Phys. Chem. C* **2011**, 115, 5545.
- [17] C. Li, Z. Y. Wu, H. W. Liang, J. F. Chen, S. H. Yu, *Small* **2017**, 13, 1700453.
- [18] S. Ye, Y. Liu, J. Feng, *ACS Appl. Mater. Interfaces* **2017**, 9, 22456.
- [19] K. Hu, T. Szkopek, M. Cerruti, *J. Mater. Chem. A* **2017**, 5, 23123.
- [20] H. Huang, P. Chen, X. Zhang, Y. Lu, W. Zhan, *Small* **2013**, 9, 1397.
- [21] H. Yang, Z. Li, B. Lu, J. Gao, X. Jin, G. Sun, G. Zhang, P. Zhang, L. Qu, *ACS Nano* **2018**, 12, 11407.
- [22] X. Cao, Z. Yin, H. Zhang, *Energy Environ. Sci.* **2014**, 7, 1850.
- [23] S. Nardecchia, D. Carriazo, M. L. Ferrer, M. C. Gutiérrez, F. del Monte, *Chem. Soc. Rev.* **2013**, 42, 794.
- [24] D. Long, J. Zhang, J. Yang, Z. Hu, G. Cheng, X. Liu, R. Zhang, L. Zhan, W. Qiao, L. Ling, *Carbon* **2008**, 46, 1253.
- [25] E. G. Calvo, E. J. Juárez-Pérez, J. A. Menéndez, A. Arenillas, *J. Colloid Interface Sci.* **2011**, 357, 541.
- [26] M. Canal-Rodríguez, A. Arenillas, N. Rey-Raap, G. Ramos-Fernández, I. Martín-Gullón, J. A. Menéndez, *Carbon* **2017**, 118, 291.
- [27] G. Ramos-Fernández, M. Canal-Rodríguez, A. Arenillas, J. A. Menéndez, I. Rodríguez-Pastor, I. Martín-Gullón, *Carbon* **2018**, 126, 456.
- [28] R. J. White, N. Brun, V. L. Budarin, J. H. Clark, M. M. Titirici, *ChemSusChem* **2014**, 7, 670.
- [29] A. Allahbakhsh, A. R. Bahramian, *Nanoscale* **2015**, 7, 14139.
- [30] M. L. Rojas-Cervantes, *J. Mater. Sci.* **2015**, 50, 1017.
- [31] N. Job, A. Théry, R. Pirard, J. Marien, L. Kocon, J. N. Rouzaud, F. Béguin, J. P. Pirard, *Carbon* **2005**, 43, 2481.
- [32] O. Czakkel, K. Marthi, E. Geissler, K. László, *Microporous Mesoporous Mater.* **2005**, 86, 124.
- [33] W. Kicinski, M. Norek, M. Bystrzejewski, *J. Phys. Chem. Solids* **2013**, 74, 101.
- [34] M. Sevilla, A. B. Fuertes, *Carbon* **2006**, 44, 468.
- [35] T. Kim, C. Jo, W. G. Lim, J. Lee, J. Lee, K. H. Lee, *Carbon* **2016**, 104, 106.
- [36] A. M. Golsheikh, N. M. Huang, H. N. Lim, R. Zakaria, *RSC Adv.* **2014**, 4, 36401.
- [37] Y. Zhu, S. Murali, M. D. Stoller, A. Velamakanni, R. D. Piner, R. S. Ruoff, *Carbon* **2010**, 48, 2118.
- [38] I. Ogino, G. Fukazawa, S. Kamatari, S. Iwamura, S. R. Mukai, *J. Energy Chem.* **2018**, 27, 1468.
- [39] Z. Sui, Q. Meng, X. Zhang, R. Ma, B. Cao, *J. Mater. Chem.* **2012**, 22, 8767.
- [40] L. Qiu, J. Z. Liu, S. L. Y. Chang, Y. Wu, D. Li, *Nat. Commun.* **2012**, 3, 1241.

- [41] J. Luo, H. D. Jang, T. Sun, L. Xiao, Z. He, A. P. Katsoulidis, M. G. Kanatzidis, J. M. Gibson, J. Huang, *ACS Nano* **2011**, *5*, 8943.
- [42] Z. M. Markovic, B. M. Babic, M. D. Dramicanin, I. D. Holclajtner Antunovic, V. B. Pavlovic, D. B. Perusko, B. M. T. Markovic, *Synth. Met.* **2012**, *162*, 743.
- [43] X. Zhang, Z. Sui, B. Xu, S. Yue, Y. Luo, W. Zhan, B. Liu, *J. Mater. Chem.* **2011**, *21*, 6494.
- [44] X. Chen, D. Lai, B. Yuan, M. L. Fu, *Carbon* **2020**, *162*, 552.
- [45] S. Long, Y. Feng, F. He, S. He, H. Hong, X. Yang, L. Zheng, J. Liu, L. Gan, M. Long, *Carbon* **2020**, *158*, 137.
- [46] Y. Cheng, S. Zhou, P. Hu, G. Zhao, Y. Li, X. Zhang, W. Han, *Sci. Rep.* **2017**, *7*, 1439.
- [47] D. Dong, H. Guo, G. Li, L. Yan, X. Zhang, W. Song, *Nano Energy* **2017**, *39*, 470.
- [48] J. Zhao, R. Pan, R. Sun, C. Wen, S. L. Zhang, B. Wu, L. Nyholm, Z. B. Zhang, *Nano Energy* **2019**, *60*, 760.
- [49] Z. Wang, X. Shen, M. A. Garakani, X. Lin, Y. Wu, X. Liu, X. Sun, J. K. Kim, *ACS Appl. Mater. Interfaces* **2015**, *7*, 5538.
- [50] M. A. Worsley, T. T. Pham, A. Yan, S. J. Shin, J. R. I. Lee, M. Bagge-Hansen, W. Mickelson, A. Zettl, *ACS Nano* **2014**, *8*, 11013.
- [51] M. Canal-Rodríguez, A. Arenillas, J. A. Menéndez, D. Beneroso, N. Rey-Raap, *Carbon* **2018**, *137*, 384.
- [52] PANalytic X'Pert Highscore Plus v3.0 software (PANalytical B.V., Almelo, The Netherlands).